






Morphology controlled performance of ternary layered oxide cathodes

Zifei Meng ^{1,2}, Xiaotu Ma ^{1,2}, Luqman Azhari ¹, Jiahui Hou ¹ & Yan Wang ¹✉

With the rapid advancement of electric vehicle technologies, ternary layered oxide cathodes in commercial Li-ion batteries have become increasingly promising due to their high energy density and low cost. However, the need for higher energy density and cell stability has posed significant challenges in their development. While various coating and doping strategies have been demonstrated to improve the rate and cycle performance of cathode materials, morphology-focused modifications of these cathodes are sometimes overlooked, despite their impact on electrochemical performance. Herein, this review focuses on the morphological relationship of cathode materials to their electrochemical performance. We summarize the effects of cathode materials morphology on Li-ion diffusion and stability. We also discuss the recent advances in the development of cathode materials with different morphologies. Finally, we present future perspectives for the design of cathode materials with optimized morphologies to promote their commercialization and fundamental research.

Lithium-ion batteries (LIB) have been societally omnipresent ever since their inception three decades ago^{1,2}. However, current and future applications are pushing the performance requirements to the point where current LIB technology will soon be insufficient; improvements in capacity, longevity, and cost reductions are needed for particularly demanding technologies such as long-range electric vehicles³ and battery-powered flights⁴. The performance of LIBs is often limited by the cathode, which is typically the most expensive component while also storing far less reversible capacity per unit weight as compared to a typical graphite anode. Therefore, improvements to the cathode are an effective way to meet these requirements, and ternary layered oxide cathodes (TLOCs) are subject to the most research and development due to their relatively high energy density and low cost⁵. TLOCs are generally comprised of the composition LiMO_2 , where M is typically a combination of transition metals and other elements such as Ni, Mn, Co, Al^{6–8}, B^{7,9}, Ta^{7,10}, and W^{5,7}. Synthesis methods, performance modification methods, failure mechanisms, and recycling methods of TLOCs have been analyzed and summarized in detail in various reviews^{11–15}; however, there is a lack of research focusing on the mechanisms of how the various cathode morphologies affect the performance of TLOCs, as morphology plays an important role in the properties of TLOCs⁷. Various microstructures have been demonstrated to either enhance reversible capacity at high charge/discharge rates or improve longevity by alleviating particle strain and resisting surface degradation.

Dense polycrystalline (PC) spherical TLOCs are widely applied in commercial production because of their high tap density, uniform particle size distribution, and high fluidity, leading to high energy density and electrode loading. However, the polycrystalline structure is also well known to develop intergranular cracks during charging at high voltage over extended cycles, which exposes additional surface areas to parasitic side reactions and subsequent secondary particle pulverization, resulting in shortened cycle life^{16–18}. Meanwhile, the randomly ordered

¹Department of Mechanical and Materials Engineering, Worcester Polytechnic Institute, 100 Institute Road, Worcester, MA 01609, USA. ²These authors contributed equally: Zifei Meng, Xiaotu Ma. ✉email: yanwang@wpi.edu

primary particles cause tortuous Li^+ diffusion pathways inside the secondary particles, resulting in long diffusion distances¹⁹. The relevant parameters that can affect the Li^+ diffusion and electrochemical stability of TLOCs are summarized in Fig. 1, and most of them can be improved by adjusting particle morphology. For Li^+ diffusion, diffusion barrier, diffusion channels, crack generation, and stability can be optimized by controlling the morphology of TLOCs, while for stability, stress caused by phase transformation, crack generation, electrolyte side effects, and transition metal dissolution also can be controlled by optimizing the morphology. Thus, to alleviate these problems, morphological strategies, including surface modification, application of core-shell structures, and secondary and primary particle morphology tuning, have been investigated and developed to resist improved Li^+ diffusion pathways or surface degradation^{7,20,21}. Furthermore, single crystal (SC) structures are investigated as a suitable particle morphology for better long-term cyclability, due to the complete absence of internal grain boundaries¹¹. The performance of SC TLOCs is also heavily dependent on their morphologies, especially in regard to enclosed facets and crystal size, which all affect Li^+ diffusion and susceptibility to surface reconstruction^{22–25}.

In this review, morphology includes secondary particle size, secondary particle shapes, inner morphology of secondary particles, primary particle size, primary particle shapes, single crystal particle size, and single crystal particle shapes. For secondary inner morphology, it includes primary particle orientation, pores distribution, and gradient structure. We focus on the mechanism of how morphology affects the electrochemical performance of TLOCs in the aspects of Li^+ diffusion and stability. First, we discuss how morphology affects Li^+ diffusion path and rate by tuning Li^+ diffusion-related parameters (Fig. 1). Second, we overview the problems leading to degradation (Fig. 1) and analyze how to solve these problems by controlling the morphology of TLOCs. Last, we discuss the challenges and our perspectives on future morphology design in the field of fundamental research, sustainability of morphology, and scale-up.

Morphology-controlled Li^+ diffusion. Li^+ diffusion plays a critical role in the rate performance of TLOCs. The diffusion time of Li^+ from the core to the surface of a particle can be influenced by the diffusion path and diffusion rate. This relationship is described using Einstein's formula: $\tau = \lambda^2/D$, where τ represents diffusion time, λ represents transverse length, and D represents the diffusivity²⁶. Therefore, D and λ are critical factors that impact Li^+ diffusion in cathode materials. As shown in Fig. 2a,

within a secondary particle, there exist various Li^+ diffusion pathways. These Li^+ diffusion pathways have different diffusion paths and diffusion rates. Ideally, Li^+ diffusion pathways should have both a short diffusion path and a fast diffusion rate to facilitate efficient Li^+ migration. The morphology of TLOCs can significantly affect their Li^+ diffusion path and rate, which will be discussed in this section.

Li^+ Diffusion path. Li^+ diffusion path refers to the pathways for Li^+ diffusing from the particle core to the surface, which includes two critical parameters: the Li^+ diffusion distance and Li^+ diffusion path. The diffusion distance represents the distance from the start point to the end point of diffusion, while the diffusion path means the actual path for Li^+ diffusing from the core to the surface of the particle. When electrolytes can diffuse into the inner part of secondary particles, like porous morphology and hollow rods, the Li^+ diffusion distance is the shortest Li^+ diffusion path because Li^+ just needs to transfer from the center to the surface of the primary particle and then diffuse into the electrolyte. When an electrolyte only can wet the surface, Li^+ needs to diffuse from the center of the secondary particle, after crossing lots of primary particles, the Li^+ can reach the surface and then diffuse into the electrolyte. The Li^+ diffusion distance will depend on the particle size while the Li^+ diffusion path will depend on particle size, path tortuosity, and the hindrances to Li^+ diffusion. In TLOCs, including secondary particles of PC TLOCs, primary particles of PC TLOCs, and SC TLOCs, their morphologies play critical roles in their Li^+ diffusion distance and length. Thus, in this section, the effects of their morphologies on their diffusion path will be discussed.

Morphology-controlled Li^+ diffusion distance. To decrease the Li^+ diffusion distance from bulk to surface, the most effective method is reducing the particle size, leading to a shorter diffusion distance. However, too small a particle size will cause some problems, like lower packing efficiency and tap density, leading to low energy density of the cell^{26,27}. Therefore, balancing the Li^+ diffusion distance and other properties is important during controlling particle size.

Meanwhile, altering the shapes of particles also can achieve short Li^+ diffusion distance by allowing more electrolyte wetting of the particles^{28,29}. Particles with 2D sheet morphology, as shown in Fig. 2b, have been studied to decrease the Li^+ diffusion distance by allowing more particles at the surface, enabling ultrafast Li^+ diffusion³⁰. Hollow rods³¹ and porous morphologies

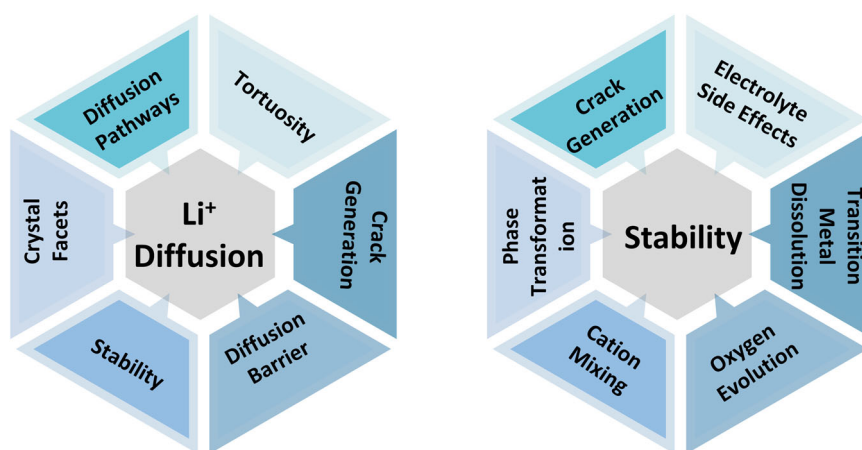


Fig. 1 Schematic depicting parameters that affect Li^+ diffusion and stability. The two images illustrate the important parameters related to Li^+ diffusion and stability, and the morphology of cathode materials can control Li^+ diffusion and stability by influencing these parameters.

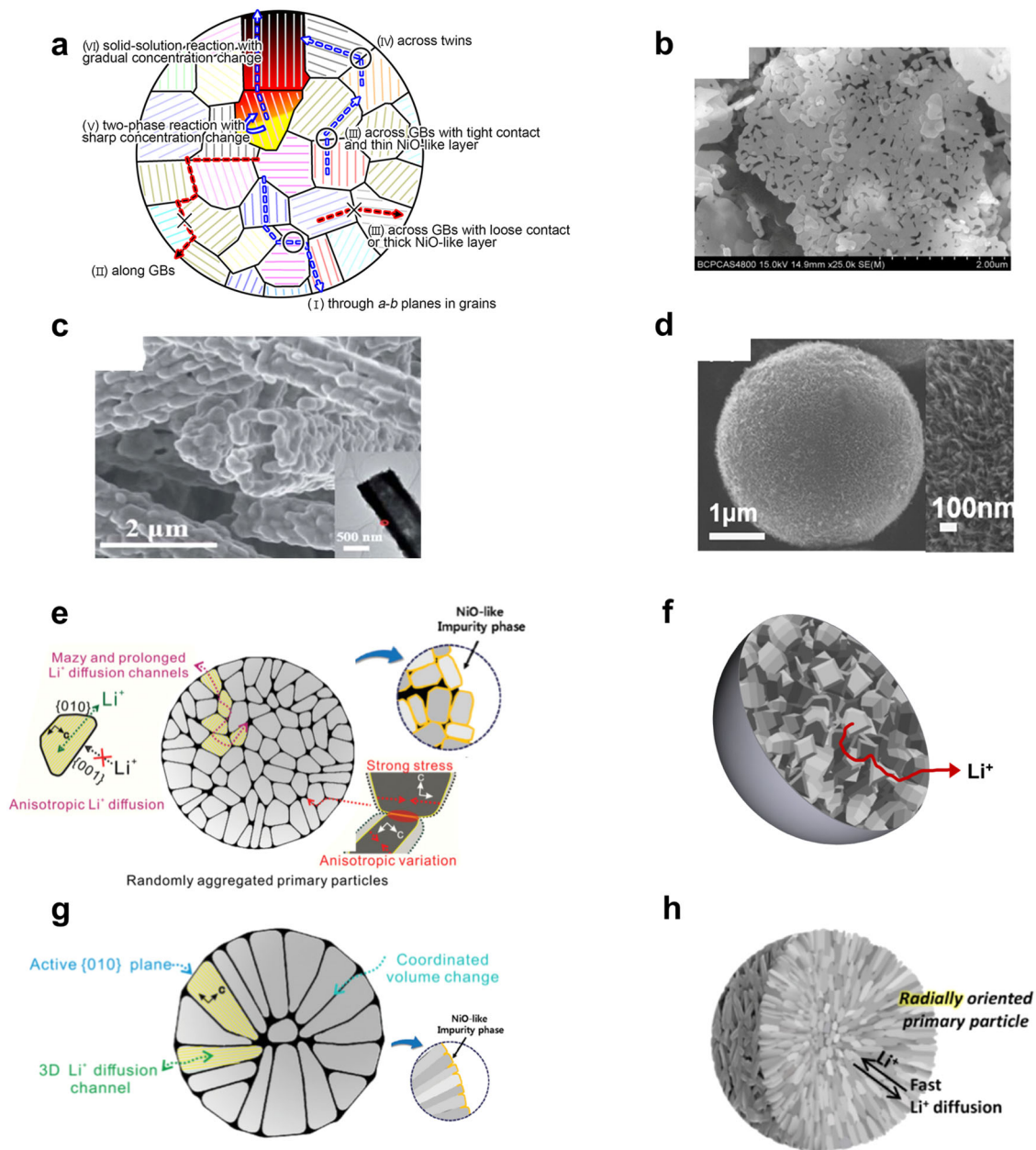


Fig. 2 The effects of morphology on the Li^+ diffusion length. **a** Schematic depicting possible and unlikely Li^+ diffusion pathways inside secondary particle: (I) shown Li^+ diffusing tortuous path through a-b planes in grains; (II) shown that Li^+ can not diffuse along grain boundaries; (III) shown that Li^+ can diffuse across grain boundaries with tight contact; (IV) shown that Li^+ can diffuse across twin grain boundaries; (V) shown that Li^+ can diffuse in sharpe concentration change area by two-phase reaction with; (VI) shown that Li^+ can diffuse through gradual concentration change area by solid-solution reaction with. **b** Scanning electron microscopy (SEM) image of a secondary particle with sheet morphology. **c** SEM image of a secondary particle with tube morphology and the inner is the TEM image of a secondary particle with tube morphology. **d** SEM image of a secondary particle with porous morphology. **e** Schematic depicting secondary particles with randomly arrogated block-like primary particles with the characterized Li^+ diffusion pathways and surface. **f** Schematic depicting secondary particles with randomly arrogated mixed primary particles with the characterized Li^+ diffusion pathways. **g** Schematic depicting secondary particles with ordered aggregated platelet primary particles with the characterized Li^+ diffusion pathways, active planes, and surface. **h** Schematic depicting secondary particles with ordered aggregated rod primary particles with the characterized Li^+ diffusion pathways. Panel **a** is adapted with permission from ref. ³⁶, Copyright American Chemical Society, 2021. Panel **b** is adapted with permission from ref. ³⁰, Copyright Royal Society of Chemistry, 2018. Panel **c** is adapted with permission from ref. ³³, Copyright Royal Society of Chemistry, 2018. Panel **d** is adapted with permission from ref. ³², Copyright Springer Nature Limited, 2016. Panel **e** and **g** are adapted with permission from ref. ¹⁹, Copyright Wiley-VCH, 2019. Panel **h** is adapted with permission from ref. ⁴¹, Copyright Elsevier, 2021.

(Fig. 2c, d) also can allow electrolytes to contact the inner particles and thus decrease the Li^+ diffusion distance^{32,33}.

Morphology-controlled Li^+ diffusion path. To achieve shorter Li^+ diffusion paths, the inner morphology of TLOCs plays a

crucial role. As shown in Fig. 2e–h, it has been observed that particles with different morphologies can have different lengths of Li^+ diffusion path, even when the diffusion distance is the same^{34–36}. This is mainly caused by the different tortuosity of Li^+ diffusion paths.

To reduce the tortuosity of Li^+ diffusion paths, controlling the orientation of primary particles and limiting the hindrances to Li^+ diffusion are effective strategies. Primary particles within the secondary particle can exhibit different crystal orientations, resulting in varying tortuosity of Li^+ diffusion pathways. Controlling the morphologies of primary particles is an effective way to organize their orientation. As illustrated in Fig. 2e, f, randomly oriented primary particles, with block-like or mixed shapes, can lead to long and winding Li^+ diffusion paths, particularly between grains with inconsistent crystal planes, due to migration across the grain boundaries¹⁹. On the other hand, as shown in Figs. 2g, h, primary particles with platelet^{34,37,38} and nanorod^{39–41} morphologies, which are aligned along (003) planes, tend to be arranged radially, providing nearly straight and the shortest Li^+ diffusion paths from the secondary particle cores to their surfaces^{7,35,38,41–44}. The longitudinal axis of nanorod primary particles is parallel to the Li^+ diffusion path, and they exhibit only slight angular deviation, thereby enabling almost straight Li^+ diffusion paths across adjacent primary particles and significantly enhancing the rate performance^{7,45–47}.

Conversely, places that impede Li^+ diffusion, such as loose contacted grain boundaries, cracks, and thick NiO-like layers on grain boundaries (Fig. 2a, e), can increase the tortuosity of Li^+ diffusion pathways³⁶. It is worth noting that these places typically develop during cycling, making the stability of particles crucial for Li^+ diffusion. Therefore, in the next section, we will discuss the relationship between stability and morphology.

Li^+ Diffusion rate. Morphology can affect not only the Li^+ diffusion path but also the Li^+ diffusion rate. The speed of Li^+ movement in the cathode material is determined by the Li^+ diffusivity (D). D can be represented through an Arrhenius relationship: $D = D_0 \exp(-\Delta G/kT)$, where D_0 represents the pre-factor determined empirically, ΔG represents the energy barrier of migration, k is the Boltzmann constant, and T is temperature⁴⁸. Therefore, changing the energy barrier for Li^+ diffusion is a critical strategy to enhance the Li^+ diffusion rate. Morphology can affect the energy barrier for Li^+ diffusion in several aspects, including grain boundaries, active area, and the distribution of crystal facets. These effects will be covered in this section.

Morphology controlled grain boundary effects on Li^+ diffusion rate. Morphology can affect the Li^+ diffusion rate by influencing grain boundary in the aspect of the grain misorientation angle. Inside TLOCs, the energy barrier for Li^+ diffusion can be influenced by whether the diffusion is through the bulk or across grain boundaries. Generally, due to the high grain boundary energy, the asymmetric grain boundaries between the primary particles are obstacles to Li^+ diffusion, which is the primary factor limiting Li^+ diffusion in TLOCs^{47,49–51}. As depicted in Fig. 3a, by decreasing the grain misorientation angle, Li^+ is easier to diffuse across the grain boundary^{36,52}. Optimal Li^+ diffusion is achieved when the transport planes are parallel to the radial direction, as shown in Fig. 3b⁵². The grain misorientation angle can be controlled by the shape and orientation of primary particles, particularly with platelet and rod shapes, the ordered orientation of primary particles can be achieved as we mentioned before, resulting in a decrease in the grain misorientation angle^{36,52,53}. Furthermore, as illustrated in Fig. 3c, SC TLOCs can provide a more continuous Li^+ diffusion pathway than PC TLOCs since they don't contain grain boundaries, and thus deliver a higher Li^+ diffusion rate.

Morphology controlled surface area effects on the Li^+ diffusion rate. The surface area is the region of the cathode particle contacting the electrolyte. Through changing the surface area of TLOCs, Li^+ diffusion rate can be controlled by morphology, because the surface area can have a significant impact on the Li^+ insertion/extraction behavior through affecting the number of active sites for Li^+ to insert and extract in a given amount of time⁵⁴. Morphology can control the surface area by the surface structures, size, and shapes of TLOCs. Although theoretically large surface area causes a high Li^+ diffusion coefficient, a very large surface area can lead to serious side reactions that can consume electrolytes and form an unstable cathode–electrolyte interface layer (CEI). These negative effects will impede the interfacial Li^+ transfer between electrolyte and TLOCs, and thus affect the Li^+ diffusion coefficient and rate performance^{55–57}. For example, in Fig. 3d, TLOCs with large grains (primary particles) deliver the best rate performance among the different sizes of grains. The main reason is that TLOCs with large surface area have high surface energy, leading to serious side reactions with electrolytes and forming an unstable intimate coating layer from electrolyte decomposition^{56,57} (Fig. 3e). Thus, it is critical to have a balance between limiting the side reaction and promoting Li^+ diffusion by controlling the surface area, and this can be achieved by modifying the morphology.

One way to adjust the surface area is by controlling the surface structure of TLOCs³². For instance, as shown in Fig. 2b, c, TLOCs with porous morphology can increase the surface area by generating pores on the surface or applying a hierarchical structure. The surface area can also be controlled by the size and shapes of both the whole particle (PC and SC TLOCs) and the primary particle. Commonly reported SC TLOCs are ~1–5 μm in size, while for PC TLOCs, secondary particle sizes can range from several microns to over 10 microns¹². A larger particle size results in a smaller specific surface area. With the same size, PC TLOCs with smaller primary particles deliver higher specific surface area because their surface contains more primary particles which can provide more exposed area^{9,56,57}. Due to the same reason, PC TLOCs show higher specific surface area than SC TLOCs of the same size^{27,58}. As shown in Fig. 3d, small particles deliver better rate performance than baseline and large particles since small particles have higher surface area. Additionally, compared to spherical shapes, TLOCs with other shapes, like rods, sheets, and dumbbells, can also increase the surface area, as the spherical shape has the smallest surface area compared to other shapes with the same volume^{59,60}. However, a large surface area may cause low capacity due to the serious side reaction. For example, although particles with sheet morphology can deliver a larger surface area than particles with spherical morphology, their capacity of them is lower, as shown in Table 1.

Morphology controlled distribution of crystal facets effects on Li^+ diffusion rate. The morphology of TLOCs can control the Li^+ diffusion rate by changing the distribution of crystal facets because different crystal facets have different Li^+ diffusion channels⁶¹ (Fig. 3f). TLOCs have the $\alpha\text{-NaFeO}_2$ layered structure, and the only channel for Li^+ diffusion is the 2D lithium layer plane. In PC TLOCs, primary particles normally have random block-like shapes, exposing (001) plane^{7,19,35,62}. The Li^+ insertion/extraction can be impeded when (001) facets, without Li^+ diffusion channels, are randomly exposed, leading to a low Li^+ diffusion rate^{61,63}. Compared to (001) facets, other facets contain more open Li^+ diffusion channels^{19,34,64}. Therefore, to improve the Li^+ diffusion rate, more crystal facets with open Li^+ diffusion channels are expected to be exposed by controlling the morphology of primary particles. For example, nanorod primary particles can make secondary particles

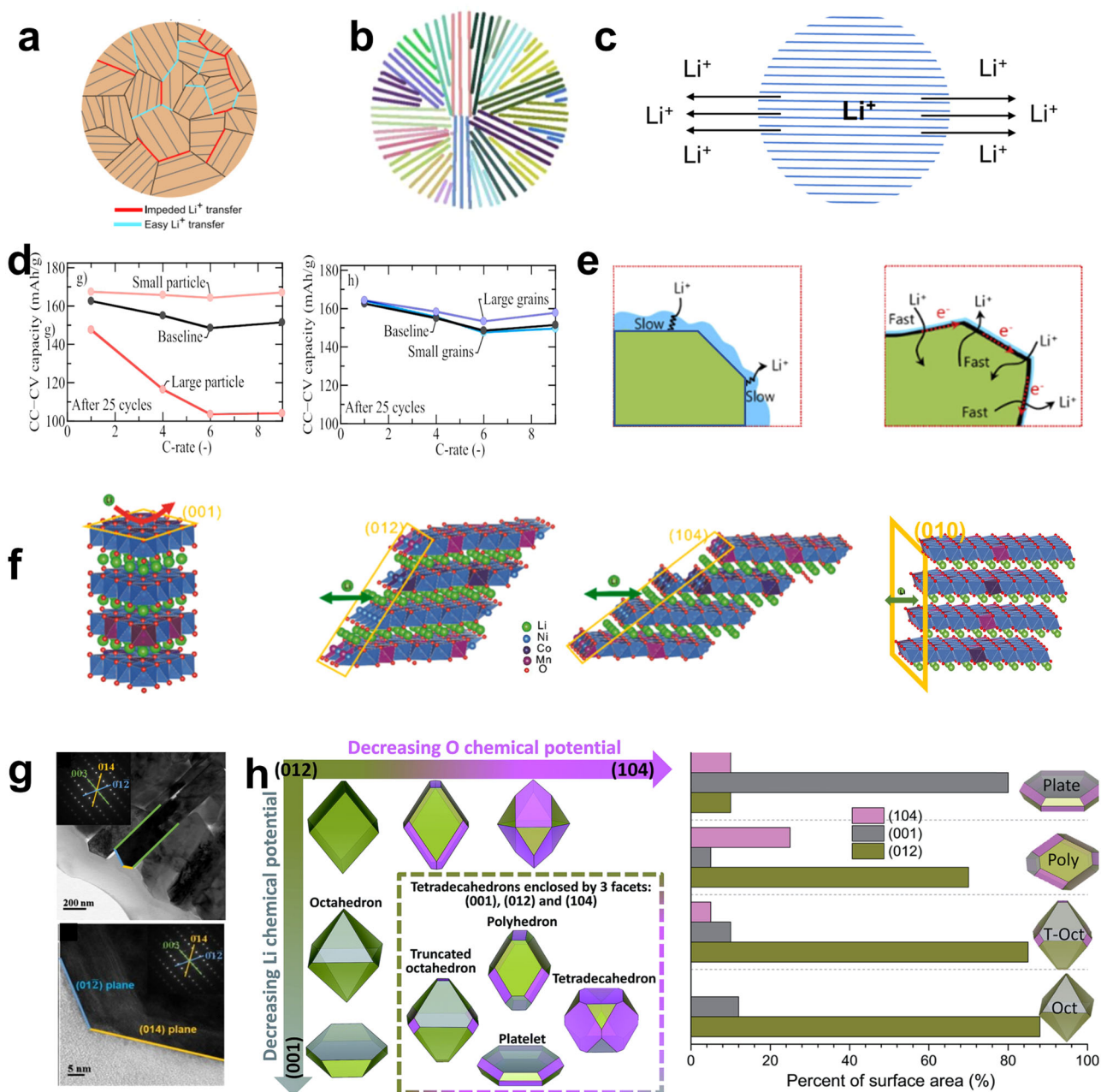


Fig. 3 The effects of morphology on Li⁺ diffusion rate. **a** Schematic depicting difficulties of Li⁺ across grain boundaries with different grain misorientation angles. **b** Schematic depicting the best case for Li⁺ across grain boundaries. **c** Schematic depicting the case for Li⁺ to diffuse inside an SC particle. **d** The rate performance of secondary particles with different particle(secondary particle) sizes and secondary particles with the same secondary particle size but different grain(primary particle) sizes. **e** The schematic of cathode–electrolyte interface layer (CEI) and Li⁺ diffusion rate on stable and unstable particle surface. **f** The schematic of the (001), (012), (104), and (010) facets. **g** Transmission electron microscopy image of primary particle exposing (012) and (104) plane on the surface of secondary particle. **h** The schematic of the presence and percentage of (012), (001), and (104) facets on the surface of SC particles with different morphologies. Panel **a** and **b** are adapted with permission from ref. ⁵², Copyright Elsevier, 2020. Panel **c** is adapted with permission from ref. ⁸⁰, Copyright Elsevier, 2020. Panel **d** is adapted with permission from ref. ²⁷, Copyright Elsevier, 2021. Panel **e** is adapted with permission from ref. ⁸¹, Copyright Elsevier, 2015. Panel **f** is adapted with permission from ref. ⁶¹, Copyright Elsevier, 2022. Panel **g** is adapted with permission from ref. ⁸, Copyright Elsevier, 2020. Panel **h** is adapted with permission from ref. ²⁵, Copyright Royal Society of Chemistry, 2019.

expose (104) crystal facets on the surface, as shown in Fig. 3g, and thus can provide more Li⁺ diffusion channels⁸. Similarly, as shown in Fig. 2g and Table 1, controlling the surface with the electrochemically active (010) planes can result in radially oriented primary particles, and thus 3D Li⁺ diffusion paths can be created, enabling Li⁺ diffuse along the active planes and straightforwardly from the center to the surface without crossing grain boundaries, significantly improving the Li⁺ diffusion rate¹⁹.

For SC TLOCs, the morphologies include nanorods^{45,65–68}, platelets^{69–73}, octahedron^{72,74,75}, tetradecahedron⁷⁶, and truncated octahedron²⁵. Their morphologies also play important roles in controlling Li⁺ diffusion rate since particles with different morphologies have different distributions of crystal facets. According to experiment and density functional theory calculation, (001), (012), and (104) crystal facets are crucial in determining the equilibrium particle shapes^{25,77}. As shown in

Table 1 Electrochemical performance and Li⁺ diffusion coefficient of PC TLOCs with different morphologies.

Type	Materials	Cutoff voltage (V)	Discharge capacity (mAh g ⁻¹)	Cycle retention (%)	Li ⁺ diffusion coefficient (cm ² s ⁻¹)	Ref.	
Normal spheres (block-like primary particles)	NMC111	2.7-4.3(rate) 3.0-4.3(cycle)	163 (0.1 C) -120 (5 C)	92.4 (200cycles 0.5 C)	10 ⁻¹¹	63	
	NMC622	2.7-4.3(rate) 3.0-4.3(cycle)	187 (0.1 C) -150 (5 C)	85.1 (100cycles 0.5 C)	10 ⁻⁹ –10 ⁻¹⁰	63	
	NMC811	2.7-4.3(rate) 3.0-4.3(cycle)	203 (0.1 C) -175 (5 C)	70.2 (100cycles 0.5 C)	10 ⁻⁸ –10 ⁻⁹	63	
Rods	NMC111	2.7-4.3	200.4 (0.1 C) 135.3 (5 C)	94 (100cycles 1 C)	1.8*10 ⁻¹⁰	46	
	NMC622	3.0-4.3	184 (0.1 C) 142 (5 C)	95.1 (100cycles, 1 C) 82.4 (1000cycles, 1 C)	3*10 ⁻⁸	29	
	NMC811	2.8-4.4	258.7 (0.1 C) 140 (5 C)	95.1 (100cycles, 1 C)	-	45	
Hollow	Rods	NMC111	2.8-4.3	163.3 (0.1 C) 142 (5 C)	97.6 (100cycles, 1 C)	-	31
		NMC622	2.8-4.3	185.6 (0.2 C) 151.6 (5 C)	94.2 (100cycles, 0.5 C)	-	33
		NMC811	2.8-4.3	194.2 (0.2 C) -150 (5 C)	87.4 (100cycles, 0.5 C)	7.86*10 ⁻⁷	33
	Spheres	NMC111	2.5-4.6	187.1 (0.1 C) 114.2 (5 C)	70.6 (200cycles, 0.5 C)	4.45*10 ⁻⁸	108
		NMC622	2.8-4.4	191.3 (0.2 C) 161.7 (5 C)	79.3 (300cycles, 1 C)	-	106
		NMC811	2.7-4.3	218.4 (0.1 C) 171.41 (5 C)	82.36 (100cycles, 0.1 C)	1.66*10 ⁻⁹	54
Sheet	NMC532	2.7-4.3	168.6 (0.1 C) 134.1 (5 C)	-90 (100cycles, 0.1 C)	-	30	
	NMC622	2.7-4.3	184.5 (0.1 C) 149.6 (5 C)	-90 (100cycles, 0.1 C)	-	30	
	NMC811	2.7-4.3	198.6 (0.1 C) 162 (5 C)	-90 (100cycles, 0.1 C)	-	30	
Core-shell spheres	CS-NMC(Ni0.74)	3.0-4.3	188 (0.1 C)	98 (500cycles, 1 C)	-	98	
	CS-GS-NMC(Ni0.68)	3.0-4.4	209 (0.5 C, 5°C)	96 (50cycles, 0.5 C)	-	100	
Primary particles	Platelet	NMC111	2.5-4.2	-175 (0.5 C) -110 (5 C)	82 (100cycles, 1 C)	7.8*10 ⁻¹⁰	37
		NMC622	3.0-4.3	180.6 (0.1 C) -120 (5 C)	86.9 (100cycles, 1 C)	10 ⁻¹⁰ –10 ⁻¹³	34
		NMC811	2.8-4.3	192.5 (0.2 C) 166.32 (5 C)	95.9 (100cycles, 0.2 C)	10 ⁻¹¹ –10 ⁻¹²	38
		NMC811	3.0-4.3	197.9 (0.1 C) 152.7 (5 C)	95.5(300cycles, 1 C)	10 ⁻⁹ –10 ⁻¹⁰	19
	Rod	NMC(Ni0.54)	2.7-4.3	183.7(0.1 C)	93.2(100cycles, 0.5 C)	-	39
		NMC(Ni0.85)	2.7-4.3	222 (0.1 C)	93.5 (100cycles, 0.5 C)	-	40
		NMC9055	2.7-4.4	235 (0.1 C) -200 (5 C)	87.9 (100cycles, 0.5 C)	-	41
	Mixed	NMC622	2.8-4.3	176 (0.1 C)	92 (50cycles, 0.5 C)	-	35

Fig. 3h, SC particles with different morphologies exhibit distinctive distributions of these crystal facets. Therefore, altering the morphologies of SC particles can modify the distribution of these crystal facets, thereby influencing the Li⁺ diffusion and rate performance, as shown in Table 2. For example, tetradecahedron SC NMC811 with (104) crystal facets delivers 169 mAh g⁻¹ discharge capacity, 10 mAh g⁻¹ and 36 mAh g⁻¹ higher than octahedron NMC811 with (012) crystal facets and PC NMC811, respectively⁷⁶. Similar results can also be found in LiNiO₂, and other types of cathode materials, so more research about modification of the distribution of crystal facets by controlling morphology is expected^{78,79}.

Morphology controlled stability. The morphology of TLOCs is a critical factor that has significant effects on stability. One key

consideration is the particle size and shape of primary, secondary, and SC TLOCs, as these characteristics can influence the mechanical stress and strain experienced by TLOCs during charging and discharging cycles. Variations in particle size and shape can result in different levels of cracking and structural degradation of TLOCs, which in turn can impact the capacity, energy density, and cycle life. Additionally, the surface area and porosity of the TLOCs can impact Li⁺ diffusion within TLOCs, which has been discussed in the section “Morphology controlled Li⁺ diffusion”. Although the surface area and porosity can affect the overall electrochemical performance, it is important to note that high surface area and porosity can also increase the likelihood of unwanted side reactions between the TLOCs and electrolytes, which can negatively impact the stability during cycling. Thus, optimizing the morphology of TLOCs is crucial for achieving high-performance and stable TLOCs. In this part, the

Table 2 Electrochemical performance and Li^+ diffusion coefficient of SC TLOCs with different morphologies.

Type	Cathode materials	Dominated facets	Cutoff voltage (V)	Discharge capacity (mAh g^{-1})	Cycle retention (%)	Li^+ diffusion coefficient ($\text{cm}^2 \text{s}^{-1}$)	Ref.
Nanorods	NMC111	001	2.8–4.6	201.2 (0.1C) 100.5 (5C)	90.2 (200cycles) 0.5C	1.43×10^{-12}	65
	NMC622	001	2.8–4.3	175.5 (0.1C) 102.5 (5C)	84.4 (100cycles) 1C	-	66
	NMC811	001	2.8–4.3	226.9 (0.1C) 140 (5C)	95.1 (100cycles) 1C	-	45
	NMC622	010	2.8–4.4	188.2 (0.1C) 128.4 (5C)	95.4 (100cycles) 0.33C 93.4 (100cycles) 2C	4.6×10^{-8}	67
Platelet	NMC(Ni0.9)	010	2.8–4.3	225 (0.1C) 156 (5C)	95.1 (100cycles) 0.2C 95.6 (100cycles) 5C	2.3×10^{-10}	68
	NMC111	010	2.5–4.6	179.2 (1C) 151.3 (5C)	89 (100cycles) 2C	-	70
	NMC111	001	3.0–4.6	157 (0.1C)	-	-	25
	NMC622	001	3.0–4.3	150 (0.1C)	70 (100cycles) 0.1C	-	71
	NMC622	001	3.0–4.6	175 (0.1C)	51 (100cycles) 0.1C	-	72
	NMC622	001	2.8–4.3	180 (0.1C)	87 (80cycles) 1C	-	72
	NMC622	001	2.8–4.3	183 (0.1C) -150 (5C)	94 (300cycles) 1C	-	69
	NMC(Ni0.91)	Unknown	3.0–4.3	203.8 (0.1C) 157.9 (4C)	80.8 (70cycles) 0.5C	-	73
	NMC111	Unknown	2.8–4.4	160 (0.1C)	-	-	74
	NMC622	Unknown	2.8–4.3	183 (0.1C) 150 (5C)	96 (80cycles) 1C	-	72
Octahedron	NMC811	012	2.8–4.5	199 (0.1C) 125 (5C)	-62.5 (100cycles) 0.5C	-	55
	NMC811	012	3.0–4.3	200 (0.1C) 159 (6C)	91.2 (100cycles) 1C	-	76
	NCA(Ni0.8)	Unknown	2.8–4.3	195 (0.2C) 158 (5C)	88 (200cycles) 1C	10^{-10} – 10^{-11}	75
	NMC811	104	3.0–4.3	200 (0.1C) 169 (6C)	93.7 (100cycles) 1C	-	76
Truncated octahedron	NMC111	012	3.0–4.3	125 (0.1C)	94.1 (100cycles) 6C	-	25
	NMC532	012	3.0–4.3	127 (0.1C)	85 (25cycles) 0.1C	-	25
	NMC811	012	3.0–4.3	190 (0.1C)	90 (60cycles) 0.1C 50 (25cycles) 0.1C	-	25

discussion of stability is focused on cycling stability, which can be affected by morphology and structure degradation. Morphology degradation is related to stress release, and tolerance, while structure degradation involves phase degradation caused by side reaction between cathode surface and electrolyte.

Stress release and tolerance. Cracks, including intergranular fracture and intragranular fracture, play a significant role in the capacity fading of TLOCs. Such cracking phenomenon has been widely discussed in the literature, and Yin et al.⁸² summarized the mechanism of microcrack formation and evolution recently. In brief, it is widely accepted that cracks are caused by phase transformation, cation mixing, lattice oxygen loss, lattice collapse, surface reconstruction, and heterogeneous lithiation/delithiation, leading to the disintegration, pulverization of particles⁸³ and decreased thermal stability, structural stability and cyclic stability of TLOCs⁸². Hence, many works focused on coating, doping, and grain boundary modification to suppress the generation of microcracks. However, the effects of morphology design have been underestimated. Morphology design can play a significant role in reducing the impact of cracks by facilitating stress release and increasing strain tolerance. This is because the stress change caused by volume fluctuations during charging and discharging can be addressed through careful optimization of the particle size, shape, porosity, and element distribution. As such, morphology design can significantly contribute to reducing the negative impact of cracks on the durability and reliability of TLOCs.

Morphology effects on heterogeneous stress. Heterogeneous stress, generated from the electrochemical expansion and contraction during charging/discharging, is the main reason for forming inter and intragranular cracking of particles⁸⁴. In particular, large particle size and random grain orientations are thought to exacerbate these cracks because large particle size can cause heterogeneous stress, which is generated from inhomogeneous delithiation/lithiation during the charging and discharging process, and random grain orientations may bring huge internal stress between primary particles. Normally, small particle size experiences low stress, because the Li concentration is more uniform in smaller particles during lithiation and delithiation⁸⁵. In particular, Cheng et al.⁸⁶ found that by decreasing particle size, tensile stress may be reduced in magnitude or even be reverted to compressive stress. However, very small particles compromise ionic partial conductivity and ionic percolation on the cathode level. Considering the more reaction between small particles and electrolytes due to the large surface area, there must be an optimum particle size⁸⁷.

Then, to further improve stress release and tolerance, researchers turned to modifying the morphology of primary particles, as shown in Fig. 4a and Table 1. Lin et al.⁴⁷ clarified primary particles' morphologies into two types: equiaxed and radially elongated morphologies. Compared to equiaxed primary particles, radially elongated primary particles have better stability and mechanical properties because they can uniformly dissipate the mechanical strain caused by internal structural changes via stacked in order along the radial direction. This radial morphology, including platelet and nanorod morphologies, can be obtained by adjusting coprecipitation reaction conditions, like pH, ammonia concentration³⁵, surfactant^{35,43}, and atomic doping⁴⁷. Radially aligned primary particles can reduce the cation mixing and alleviate the volume change caused by stress concentration during reversible Li⁺ de/intercalation, leading to better stability⁴⁷. Xu et al.¹⁹ synthesized NMC811 spherical secondary particles with radially aligned primary particles by a modified coprecipitation reaction. The radial primary particles

with consistent crystal orientation can alleviate the volume-change-induced intergranular stress by coordinated expansion and contraction, as shown in Fig. 2e, leading to less pulverization of secondary particles and improved cycling stability (without any visible degradation after 300 cycles). Introducing different doping elements, such as B^{7,8}, Ta^{7,88}, Sb⁸⁹, W^{7,90-93}, Sn⁴¹, Mo⁹⁴, and more⁹⁵, can also obtain radially aligned primary particles. Although all of these research claimed the improvement in stability, they all used equiaxed primary particles as a control group. There are no studies on how these doping strategies improve the stability of pristine spherical secondary particles with radially aligned primary particles.

Another essential factor affecting stability is the Ni content, which inherent structural instability caused by anisotropic lattice contraction in the deeply charged state generates local stress concentrations along the grain boundaries^{17,96}, when the fraction of Ni is increased. Herein, core-shell morphology has been studied in abundant research articles, since it can reduce the internal stress concentration, as shown in Fig. 4b and Table 1. By employing core-shell morphology, the Mn/Co-rich shell could improve the mechanical properties⁹⁷ and provide pressure to the inner core, which will be balanced by the tensile stress⁸². For example, core-shell TLOCs with a [Ni_{0.8}Co_{0.1}Mn_{0.1}](OH)₂ core and [Ni_{0.5}Mn_{0.5}](OH)₂ shell are designed to simultaneously ensure structural and thermal stability⁹⁸. In comparison with NMC811, the core-shell structure exhibited a lower discharge capacity but enhanced cyclability, retaining 17% more of its capacity than that of NMC811 (1 C, 3.0-4.3 V) after 500 cycles⁹⁸. Besides, Liu et al.⁹⁷ studied the effects of Co and Mn on the mechanical properties of Ni-rich TLOCs, which provide guidelines for the design of core-shell TLOCs. As shown in Fig. 4c, their work revealed that the Co-enriched surface design benefits from its low stiffness, which can suppress the generation of particle cracks. Meanwhile, the Mn-enriched core limits internal expansion and improves structural integrity.

However, the compositional mismatch between core and shell is difficult to prevent, especially during intercalation, and the interface is susceptible to crack and reduction of the lithium-ion transport efficiency from the core⁹⁹. To overcome these challenges, the core-shell morphology evolved to core-shell concentration gradient¹⁰⁰, then to full concentration gradient^{40,101,102}. Combining them with primary particle morphology modification can further improve the stability^{100,102-104}. Nevertheless, due to the morphological similarity between the full gradient strategy and the conventional spherical secondary particle, an extensive discussion of the former will not be pursued at this time. Although core-shell and full gradient morphology exhibit impressive performance and stability, they are still limited by their repeatability and consistency for scaled-up¹⁰⁵.

Morphology effects on intergranular stress. Handling intergranular stress is also a potential strategy to improve the mechanical properties of TLOCs from morphology, which can be achieved by reserving space to accommodate volume change or removing grain boundaries. Thus, porous³², hollow¹⁰⁶, and SC morphologies have been developed, and they show better cycle stability than unmodified TLOCs, as shown in Table 1.

Porous and hollow morphologies can be obtained by coprecipitation reaction¹⁰⁷ and sacrificial templates method^{32,108}. Porous NMC111 exhibited excellent rate and cycle performance at high voltage^{32,109}. Porous morphology increases the surface area and decreases the length of the diffusion pathway¹¹⁰, which makes lithiation and delithiation more efficient, leading to a homogeneous delithiation and uniform stress generation during

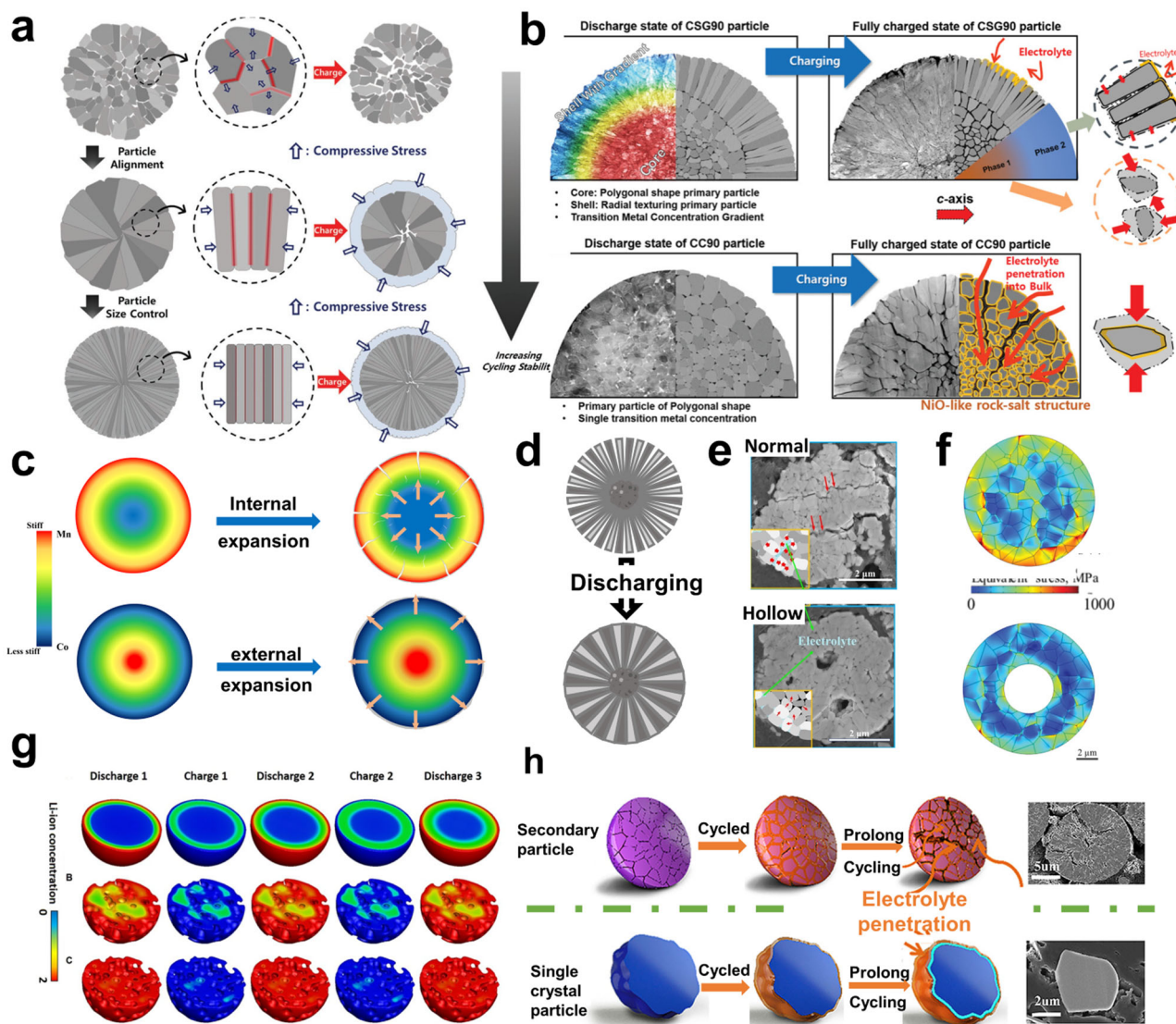


Fig. 4 The effects of morphology on stress release and tolerance. **a** The schematic of a build-up of local stress concentrations and stress distribution during charging depending on primary particle morphology. **b** The schematic of different degrees of sustained damage because of the different morphology. **c** The schematic of concentration gradient designs with Co-rich or Mn-rich surface and their mechanical stability. **d** The schematic of porous morphology. **e** SEM image of hollow microspheres. **f** The finite element modeling of the equivalent stress within the normal and hollow NMC particles upon completion of charging. **g** Cross-sectional image of the Li^+ concentration at the completion of each discharging and charging process in a spherical cathode with 0%, 20%, and 50% porosity, respectively (C-rate is 40 C). **h** The schematic of crack evolution and the internal morphological difference for PC and SC particles during prolonged cycling. Panel **a** is adapted with permission from ref. ⁹, Copyright Wiley-VCH, 2020. Panel **b** is adapted with permission from ref. ¹⁴², Copyright Wiley-VCH, 2019. Panel **c** is adapted with permission from ref. ⁹⁷, Copyright Springer Nature Limited, 2021. Panel **e** is adapted with permission from ref. ¹⁴³, Copyright Wiley-VCH, 2019. Panel **f** is adapted with permission from ref. ¹⁴⁴, Copyright Wiley-VCH, 2019. Panel **g** is adapted with permission from ref. ¹¹⁰, Copyright Springer Nature Limited, 2017. Panel **h** is adapted with permission from ref. ¹⁴⁵, Copyright Elsevier, 2020.

the charging/discharging process for suppressing cracks formation (Fig. 4d–g). Due to the same reason, as shown in Fig. 4e, hollow microspheres can also deliver a homogeneous delithiation and thus improve the rate and cycle performance; at 5 C, the capacity difference between hollow spherical NMC111 and normal spherical NMC111 was over 60 times. A similarly produced hollow NMC111 exhibited a capacity retention improvement of almost 30% after 150 cycles (1 C, 2.8–4.45 V) (ref. ¹¹¹). Furthermore, Liu et al.¹¹² analyzed the advantages of hollow morphology on stress reduction and Ma et al.¹¹³ showed that larger voids can alleviate stress concentration and more porous can lower tensile hoop stress (Fig. 4g). However, porous and hollow morphology will lead to a low tap density, resulting in low volume energy density.

SC morphology is an important advance in improving stability through morphology engineering. SC morphology eliminates the intergranular cracks due to the grain boundaries-free structure (Fig. 4h). Compared to intergranular cracks, the intragranular cracks have less influence on stability, thus the cycle stability of SC NMC622 is over 30% better than that of the PC NMC622⁶⁹. Meanwhile, the intergranular cracks could be reduced by adjusting the orientation of the main crystal plane in SC TLOCs. Zhu et al. found that it could enhance stability by replacing the active (012) crystal face with inactive (001) or (104) planes²⁵. In addition, SC particles exhibit higher mechanical strength than PC particles. Cha et al. found that SC particles can maintain their original morphology from 15 to 45 MPa and they have homogeneous reactivity during the charging and discharging

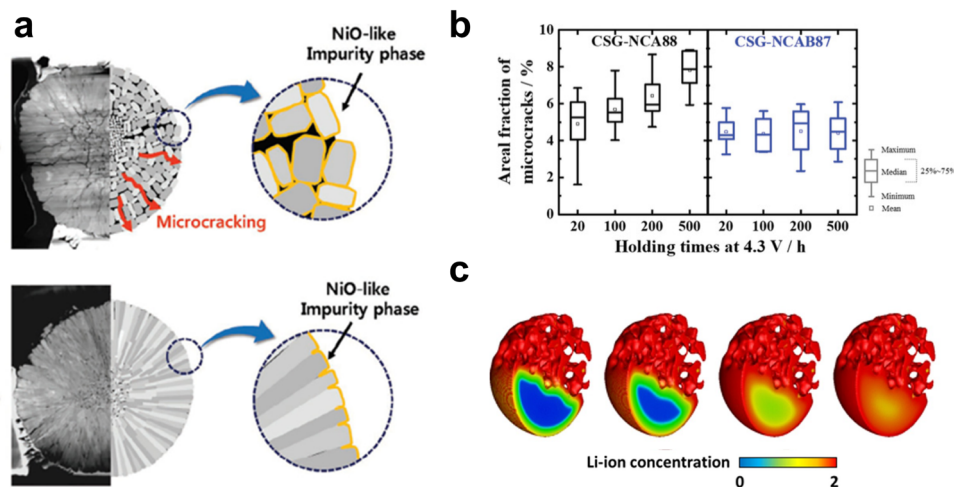


Fig. 5 The effects of morphology on surface stability. **a** The schematic of the effects of primary particle shapes on the chemical stability of the cathode surface during charge and discharge cycling. **b** Areal fraction of microcracks of secondary particles with different morphologies of primary particles in the charged state after different holding times at 4.3 V (The bars represent the statistical distribution of values). **c** Cross-sectional image of the Li^+ concentration in the particle with 40% porosity and an uneven distribution. Panel **a** is adapted with permission from ref. 88, Copyright Wiley-VCH, 2018. Panel **b** is adapted with permission from ref. 123, Copyright Wiley-VCH, 2022. Panel **c** is adapted with permission from ref. 110, Copyright Springer Nature Limited, 2017.

process¹¹⁴. Overall, SC morphology eliminates the intragranular cracks and provides high mechanical properties and high cycle stability as shown in Table 2, however, it is limited by the control of morphology and size.

Other morphology designs effects on stability. There are other shapes of TLOCs, like rods^{31,115,116}, wires²⁹, sheet^{28,30,117}, fibers¹¹⁸, and ellipsoidal¹¹⁹. They are attractive morphologies since they allow both Li^+ ions and electrons to be inserted feasibly, facilitating high ionically and electronic conductivities simultaneously, but also large surface-to-volume ratios. Mixed metal oxalate micro rods can be regarded as precursors via a two-step coprecipitation reaction to prepare microrod $\text{LiNi}_{0.8}\text{Co}_{0.15}\text{Al}_{0.05}\text{O}_2$ (ref. 116). The obtained microrod TLOCs exhibit a 6% better capacity retention after 100 cycles at 1 C. Hollow micro rods of NMC811 and NMC111 with high performance can be synthesized by adjusting the coprecipitation reaction^{31,33}. In one work, CoC_2O_4 was chosen to precipitate first because its growth preference into nanorods can be utilized as a template during the precipitation of the other transition metal (TM) elements. In another work, nanofiber NMC622 with good performance was fabricated by ultrasound-triggered cation chelation and reassembly route²⁹. However, these results lack the comparison with commercial PC TLOCs. And few studies have reported their mechanical properties. Stein et al. revealed the distributions of stresses in ellipsoidal particles, which are lower than spherical particles because the stresses were equilibrated by deformations along the semi-major axis¹¹⁹. Deshpande et al. only studied the diffusion-induced stress in nanowire morphology without comparison with other morphologies¹²⁰. Therefore, there is still abundant work for other shapes development. Furthermore, the scale-up, repeatability, and consistency are also important for these morphologies.

Surface stability. Since the reaction between TLOCs and electrolytes at high states of charge leads to mechanical instability, reducing the surface area exposed to electrolytes and preventing parasitic electrolyte attack is important to reduce the accumulation of NiO-like impurity layers at the cathode–electrolyte interface⁸², which could be achieved by morphology modification, as shown in

Fig. 5a. However, the good contact between cathode and electrolyte could benefit the Li diffusion, leading to better rate performance and less heterogeneous stress. Thus, there should be a balance for the contact between the cathode and electrolyte.

Morphology-controlled surface area effects on surface stability.

The particle size can directly affect the surface area of cathode particles. As reducing the particle size of TLOCs, the increased surface area is more prone to surface reaction and particle dissolution in the electrolyte, resulting in a severe reduction in the cyclic life of TLOCs¹²¹. Li et al. reported that large $\text{LiNi}_{0.7}\text{Co}_{0.15}\text{Mn}_{0.15}\text{O}_2$ cathode particles had an enhanced cycle performance benefited by smaller surface area and thick CEI layer¹²².

The modification of primary particles can also affect the stability of TLOCs by influencing the contact between the cathode and electrolyte. As shown in Table 1, this method can significantly improve the stability. The tight accumulation of elongated primary particles could reduce the contact with the electrolyte⁴⁷. Namkoong et al. investigated the effect of exposure time to the electrolyte on the TLOCs at a high state of charge. In this work, as shown in Fig. 5b, the TLOCs with radially elongated primary particles show less exposure time owing to the suppression cracks generation by radially primary particle morphology, which reduces the contact between the new exposure surface and electrolyte¹²³.

Morphology-controlled surface protection.

Core-shell morphology with full concentration gradient reduced the contact between Ni^{4+} ions and electrolytes by reducing the content of Ni on the surface, as shown in Fig. 4b. The high content of Ni^{2+} and Mn-rich surface suppresses the reaction from Ni^{2+} to Ni^{4+} , resulting in less reaction between Ni^{4+} and electrolyte^{100,102} and the improved stability. In addition, since SC morphology eliminates the intergranular fractures, the amount of new surface exposure to the electrolyte is significantly reduced, as shown in Fig. 4h, which prevents contact between the new surface and electrolyte⁸². Furthermore, porous, hollow, and other morphologies always provide a high surface area. Hence, it was of great importance to determine the optimal porosity. Song et al. investigated the effects of pore distribution in the spherical

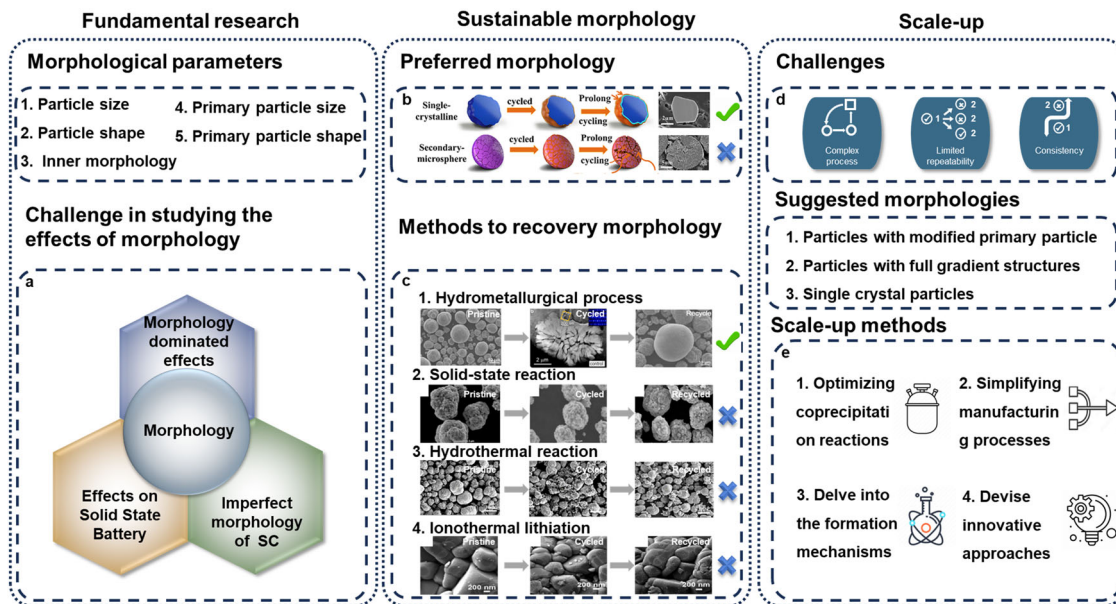


Fig. 6 The summary and perspective of the effects of morphology. **a** The schematic of challenge in studying the effects of morphology. **b** The schematic of preferred single crystal morphology for sustainability (crack evolution and the internal morphological difference for PC and SC particles during prolonged cycling). **c** SEM image of morphology of pristine, cycled, and recycled cathode materials from the hydrometallurgical process, solid-state reaction, hydrothermal reaction, and ionothermal lithiation. **d** The challenges for scale-up. **e** The methods for scale-up. Panel **b** is adapted with permission from ref. ¹⁴⁵, Elsevier, 2020. Panel **c** is adapted with permission from ref. ¹¹³, Copyright Elsevier, 2021, ref. ¹²⁷, Copyright American Chemical Society, 2022, ref. ¹⁴⁶, Copyright Elsevier, 2022, and ref. ¹⁴⁷, Copyright Wiley-VCH, 2020.

TLOCs¹¹⁰, and they stated that if the pores are not evenly distributed, the performance could decrease with increasing porosity, as shown in Fig. 5c. Thus, how to balance both stability and surface area by morphology control have not been fully studied. Controlling both particle size and percentage of different crystal facets at the same time might be a possible solution, and more theoretical calculations, as well as experiments in this field, are needed.

Summary and perspective. The morphological configuration of TLOCs plays a critical role in determining the performance of LIBs. In this paper, we discuss the effects of morphological design on Li⁺ diffusion and mechanical properties which exhibit the significant potential to affect the capacity and stability of TLOCs. By modifying the morphology, the Li⁺ diffusion path and rate can be altered, leading to distinct rate performance characteristics. Furthermore, an optimal morphology can effectively alleviate and withstand the stress induced by volume changes during the charging and discharging processes. Nevertheless, it is widely acknowledged that a trade-off relationship exists between rate and cycle performance, which extends to the domain of morphology design. Consequently, researchers must strike a delicate balance in their morphology design efforts to achieve desirable rate and cycle performance characteristics.

Hence, we believe that future morphology design could be further developed from the following aspects: (1) fundamental research; (2) sustainable morphology; and (3) scale-up. The relevant concepts are summarized in Fig. 6. First of all, the function of morphology should be clarified in fundamental research. For example, morphology parameters are always ignored in the study of coating and doping for Ni-rich TLOCs. The absence of essential morphological properties, including particle size, BET surface area, and porosity, in various articles could potentially explain the observed discrepancies in performance despite employing similar coating or doping strategies. Moreover, the effects of primary particles' morphology are

neglected. In many published articles, researchers utilize pristine particles featuring block-shaped primary particles as the starting material for coatings or doping experiments. As a result, the morphology of the primary particles undergoes a transformation from block-shaped to rod-shaped, which has been shown to enhance both rate and cycle performance. Surprisingly, there is a noticeable absence of studies comparing the performance improvements achieved by modifying pristine particles with rod-shaped primary particles. Consequently, it remains unclear whether the changes in primary particle morphology or the effects of the coating or doping elements primarily drive the observed performance enhancements. Therefore, it is crucial to address this knowledge gap and elucidate the relative contributions of primary particle morphology and the presence of coating or doping elements to the overall performance improvements.

In addition, compared to the study of PC morphologies, SC morphology is a new strategy to improve the stability of TLOCs, especially for Ni-rich TLOCs. Thus, many morphological effects of SC TLOCs need to be explored. Up to date, all SC TLOCs are mixed with several different morphologies, which may lead to problems in electrode manufacturing and research about the function of morphology. Therefore, it is notable to study how to synthesize SC TLOCs with single morphology and whether the performance of SC TLOCs with single morphology is better than that of SC TLOCs with mixed morphologies. In addition, for SC particles synthesized from precursors, the effects of primary particles in precursor on SC morphologies have not been comprehensively investigated. As coating/doping elements have an impact on primary particles' morphology in secondary particles, their effects on SC morphology or crystal facets have not been reported. Thus, there are many puzzles that need to be addressed for SC morphology.

Besides, morphology optimization can also improve the interface between the cathode and solid-state electrolyte in all-solid-state batteries (ASSBs). The morphological effects, such as particle size, have been investigated^{124,125}. Especially, SC

morphology is a potential candidate of TLOCs for ASSBs, which can provide a better interface reaction between the cathode and solid-state electrolyte compared with PC¹²⁶. However, other morphologies of PC TLOCs, like primary particles' morphology and core-shell morphology, have not been deeply studied, which have the potential to improve the Li⁺ diffusion in the interface of cathode and solid-state electrolytes. Additionally, due to various types of solid-state electrolytes, more studies are necessary to pair different morphologies of SC and PC particles and different solid-state electrolytes.

Secondly, to achieve the target of net zero, the sustainability of cathode materials needs to be considered for reducing the cost, energy cost, and greenhouse gas emissions in the recycling processes. After cycling, the morphology of the cathode materials could be damaged, which affects the performance, quality, and consistency of electrodes, and its recovery of the morphology is often overlooked despite its importance. Different morphologies pose challenges in recycling: PC TLOCs struggle to maintain their original morphology due to cracks, while SC TLOCs are easier to recover. Based on present technologies, direct recycling, and hydrometallurgical processes offer solutions^{127–130} but each has its limitations. Direct recycling can easily recover the electrochemical performance as same as the commercial cathode materials by recovering Li content and structure with the hydrothermal^{131,132}, solid-state reaction^{133,134}, ionothermal lithiation¹³⁵, and electrochemical relithiation processes¹³⁶, but the morphology destroyed by large cracks is not able to be recovered back to perfect spheres^{137,138}. The recovered cathode exhibits an abundance of small particles (less than 5µm) with irregular shape¹³⁹ or totally irregular shape of recovered particles¹⁴⁰, which may lead to a lower tap density and casting problems in electrode manufacturing. Meanwhile, the heat treatment of direct recycling may lead to larger primary particles, even changing shapes of primary particles, resulting in worse capacity and stability. Thus, we believe that complex morphologies, such as spheres, hollows, core shells, and so on, are better suited for hydrometallurgical processes due to the resynthesis process included in this type of recycling process. Through the hydrometallurgical process, all defects in spent cathode materials can be recovered. Moreover, the recycled materials enabled better performance than the commercial cathodes^{113,141}.

On the other hand, SC morphology fits both the direct and hydrometallurgical recycling processes because of its simple morphology. SC TLOCs can be simply recovered by direct recycling because SC morphology is easier to maintain than PC morphology during cycling¹²⁸. Although the SC particles will have cracks or break into small particles as the PC TLOCs after cycling, the particle size and facets can be recovered by controlling sintering temperature, time, and different lithium salts. Also, the hydrometallurgical recycling process can recover the SC TLOCs, but the process is more complicated compared to the direct recycling process.

Finally, although there has been a growing interest in exploring new morphologies for cathode materials, such as SC morphology, the academic and industrial sectors still predominantly favor traditional spherical PC particles. This preference can be attributed to the well-established synthesis methods and electrode fabrication processes for PC materials, which have reached a high level of maturity. The hesitance to adopt advanced morphologies can be attributed to several factors, including the complexity of manufacturing processes, limited repeatability and consistency, and challenges associated with scaling up production. In light of these considerations, we would suggest that future endeavors in morphological design should concentrate on modifying the morphology of primary particles, achieving full gradient structures, and exploring SC morphologies. These morphologies can be

potentially obtained through the optimization of coprecipitation reactions, a widely utilized technique in industry. To facilitate progress in simplifying manufacturing processes, it is imperative for researchers to delve into the formation mechanisms underlying these advanced morphologies. By gaining a deeper understanding of the factors influencing the formation of advanced morphologies, it becomes possible to devise innovative approaches that enable their reliable and scalable production. This, in turn, would pave the way for the adoption of advanced morphologies in practical applications, thereby leveraging their potential benefits for enhancing the performance of lithium-ion batteries.

Received: 20 September 2023; Accepted: 20 October 2023;

Published online: 03 November 2023

References

1. Fan, X. et al. In situ inorganic conductive network formation in high-voltage single-crystal Ni-rich cathodes. *Nat. Commun.* **12**, 5320 (2021).
2. Yan, P. et al. Tailoring grain boundary structures and chemistry of Ni-rich layered cathodes for enhanced cycle stability of lithium-ion batteries. *Nat. Energy* **3**, 600–605 (2018).
3. Li, W., Erickson, E. M. & Manthiram, A. High-nickel layered oxide cathodes for lithium-based automotive batteries. *Nat. Energy* **5**, 26–34 (2020).
4. Viswanathan, V. et al. The challenges and opportunities of battery-powered flight. *Nature* **601**, 519–525 (2022).
5. Thackeray, M. M. & Amine, K. Layered Li–Ni–Mn–Co oxide cathodes. *Nat. Energy* **6**, 933–933 (2021).
6. Li, W., Lee, S. & Manthiram, A. High-Nickel NMA: A Cobalt-Free Alternative to NMC and NCA Cathodes for Lithium-Ion Batteries. *Adv. Mater.* **32**, 2002718 (2020).
7. Kim, U.-H. et al. Heuristic solution for achieving long-term cycle stability for Ni-rich layered cathodes at full depth of discharge. *Nat. Energy* **5**, 860–869 (2020). **This study provides the effects of radially aligned primary particles on dissipate the train during charge state.**
8. Ryu, H.-H. et al. A highly stabilized Ni-rich NCA cathode for high-energy lithium-ion batteries. *Mater. today* **36**, 73–82 (2020).
9. Ryu, H.-H. et al. New Class of Ni-Rich Cathode Materials Li[NixCo_{1-x}Y]O₂ for Next Lithium Batteries. *Adv. Energy Mater.* **10**, 2000495 (2020). **The effects of primary particle size and shapes on cycling stability have been studied by analysing the inner compressive stress.**
10. Yu, H. et al. Restraining the escape of lattice oxygen enables superior cyclic performance towards high-voltage Ni-rich cathodes. *Natl Sci. Rev.* **10**, nwac166 (2023).
11. Langdon, J. & Manthiram, A. A perspective on single-crystal layered oxide cathodes for lithium-ion batteries. *Energy Storage Mater.* **37**, 143–160 (2021).
12. Han, Y. et al. Single-crystalline cathodes for advanced Li-ion batteries: progress and challenges. *Small* **18**, 2107048 (2022).
13. De Biasi, L. et al. Chemical, structural, and electronic aspects of formation and degradation behavior on different length scales of Ni-rich NCM and Li-rich HE-NCM cathode materials in Li-ion batteries. *Adv. Mater.* **31**, 1900985 (2019).
14. Lv, Y. et al. A review of nickel-rich layered oxide cathodes: synthetic strategies, structural characteristics, failure mechanism, improvement approaches and prospects. *Appl. Energy* **305**, 117849 (2022).
15. Tao, Q. et al. Understanding the Ni-rich layered structure materials for high-energy density lithium-ion batteries. *Mater. Chem. Front.* **5**, 267–2622 (2021).
16. Yoon, M. et al. Reactive boride infusion stabilizes Ni-rich cathodes for lithium-ion batteries. *Nat. Energy* **6**, 362–371 (2021).
17. Ryu, H.-H., Park, K.-J., Yoon, C. S. & Sun, Y.-K. Capacity fading of Ni-Rich Li[Ni_xCo_yMn_{1-x-y}]O₂ (0.6 ≤ x ≤ 0.95) cathodes for high-energy-density lithium-ion batteries: bulk or surface degradation? *Chem. Mater.* **30**, 1155–1163 (2018).
18. Yan, P. et al. Intragranular cracking as a critical barrier for high-voltage usage of layer-structured cathode for lithium-ion batteries. *Nat. Commun.* **8**, 14101–14101 (2017).
19. Xu, X. et al. Radially oriented single-crystal primary nanosheets enable ultrahigh rate and cycling properties of LiNi_{0.8}Co_{0.1}Mn_{0.1}O₂ cathode material for lithium-ion batteries. *Adv. Energy Mater.* **9**, 1803963 (2019). **This research introduces the 3D Li⁺ diffusion channels by modifying the morphology and exposed active crystal facets of primary particles.**
20. Sun, Y.-K. et al. Nanostructured high-energy cathode materials for advanced lithium batteries. *Nat. Mater.* **11**, 942–947 (2012).

21. Jun, D.-W., Yoon, C. S., Kim, U.-H. & Sun, Y.-K. High-energy density core-shell structured Li[Ni_{0.95}Co_{0.025}Mn_{0.025}]O₂ cathode for lithium-ion batteries. *Chem. Mater.* **29**, 5048–5052 (2017).
22. Zhang, H. et al. Single-crystalline Ni-Rich LiNi_xMnyCo_{1-x-y}O₂ cathode materials: a perspective. *Adv. Energy Mater.* **12**, 2202022 (2022).
23. Cao, B., Fang, H.-T., Li, D. & Chen, Y. Controlled synthesis of single-crystalline ni-rich cathodes for high-performance lithium-ion batteries. *ACS Appl. Mater. Interfaces* **14**, 53667–53676 (2022).
24. Meng, X.-H. et al. Kinetic origin of planar gliding in single-crystalline Ni-rich cathodes. *J. Am. Chem. Soc.* **144**, 11338–11347 (2022).
25. Zhu, J. & Chen, G. Single-crystal based studies for correlating the properties and high-voltage performance of Li[NixMnyCo_{1-x-y}]O₂ cathodes. *J. Mater. Chem. A* **7**, 5463–5474 (2019). **Single crystal cathodes with different morphologies were synthesized and compared in this articles, and the relationship between morphology and crystal facets have been detailly analyzed.**
26. Lipson, A. L. et al. Improving the thermal stability of NMC 622 Li-Ion battery cathodes through doping during coprecipitation. *ACS Appl. Mater. Interfaces* **12**, 18512–18518 (2020).
27. Allen, J. M. et al. Quantifying the influence of charge rate and cathode-particle architectures on degradation of Li-ion cells through 3D continuum-level damage models. *J. Power Sources* **512**, 230415 (2021). **The capacity fading of NMC 532 with different secondary particle and primary particle size has been comprehensively studied in both theoretical simulation and experiments.**
28. Wu, T. et al. Thick electrode with thickness-independent capacity enabled by assembled two-dimensional porous nanosheets. *Energy Stor. Mater.* **36**, 265–271 (2021).
29. Lai, Y. et al. An ultrasound-triggered cation chelation and reassembly route to one-dimensional Ni-rich cathode material enabling fast charging and stable cycling of Li-ion batteries. *Nano Res.* **13**, 3347–3357 (2020).
30. Wu, Y. et al. A general strategy for the synthesis of two-dimensional holey nanosheets as cathodes for superior energy storage. *J. Mater. Chem. A* **6**, 8374–8381 (2018).
31. Yang, Z. et al. Stepwise co-precipitation to synthesize LiNi_{1/3}Co_{1/3}Mn_{1/3}O₂ hierarchical structure for lithium ion batteries. *J. Power Sources* **272**, 144–151 (2014).
32. Chen, Z. et al. Hierarchical porous LiNi_{1/3}Co_{1/3}Mn_{1/3}O₂ nano-/micro spherical cathode material: minimized cation mixing and improved Li⁺ mobility for enhanced electrochemical Performance. *Sci. Rep.* **6**, 25771–25771 (2016).
33. Chen, F. et al. Sequential precipitation induced interdiffusion: a general strategy to synthesize microtubular materials for high performance lithium ion battery electrodes. *J. Mater. Chem. A* **6**, 18430–18437 (2018).
34. Jiang, M. et al. Synthesis of Ni-rich layered-oxide nanomaterials with enhanced li-ion diffusion pathways as high-rate cathodes for Li-ion batteries. *ACS Appl. Energy Mater.* **3**, 6583–6590 (2020).
35. Yang, C.-K. et al. Insights into the inner structure of high-nickel agglomerate as high-performance lithium-ion cathodes. *J. Power Sources* **331**, 487–494 (2016).
36. Nomura, Y., Yamamoto, K., Yamagishi, Y. & Igaki, E. Lithium transport pathways guided by grain architectures in Ni-rich layered cathodes. *ACS Nano* **15**, 19806–19814 (2021). **This study analysed the possible Li⁺ diffusion pathways inside secondary particles and effects of the misorientation angles between primary particles on Li⁺ movement.**
37. Peng, L., Zhu, Y., Khakoo, U., Chen, D. & Yu, G. Self-assembled LiNi_{1/3}Co_{1/3}Mn_{1/3}O₂ nanosheet cathodes with tunable rate capability. *Nano Energy* **17**, 36–42 (2015).
38. Su, Y. et al. High-rate structure-gradient Ni-rich cathode material for lithium-ion batteries. *ACS Appl. Mater. Interfaces* **11**, 36697–36704 (2019).
39. Noh, H.-J., Ju, J. W. & Sun, Y.-K. Comparison of nanorod-structured Li[Ni_{0.54}Co_{0.16}Mn_{0.30}]O₂ with conventional cathode materials for Li-ion batteries. *ChemSusChem* **7**, 245–252 (2014).
40. Yoon, C. S. et al. High-energy Ni-rich Li[NixCoyMn_{1-x-y}]O₂ cathodes via compositional partitioning for next-generation electric vehicles. *Chem. Mater.* **29**, 10436–10445 (2017).
41. Thien Nguyen, T., Kim, U.-H., Yoon, C. S. & Sun, Y.-K. Enhanced cycling stability of Sn-doped Li[Ni_{0.90}Co_{0.05}Mn_{0.05}]O₂ via optimization of particle shape and orientation. *Chem. Eng. J.* **405**, 126887 (2021).
42. Yoon, S.-J. et al. Nanorod and nanoparticle shells in concentration gradient core-shell lithium oxides for rechargeable lithium batteries. *ChemSusChem* **7**, 3295–3303 (2014).
43. Ju, X. et al. Surfactant-assisted synthesis of high energy {010} facets beneficial to Li-ion transport kinetics with layered LiNi_{0.6}Co_{0.2}Mn_{0.2}O₂. *ACS Sustain. Chem. Eng.* **6**, 6312–6320 (2018).
44. Hou, D. et al. Effect of the grain arrangements on the thermal stability of polycrystalline nickel-rich lithium-based battery cathodes. *Nat. Commun.* **13**, 3437 (2022).
45. Guo, F., Xie, Y. & Zhang, Y. Low-temperature strategy to synthesize single-crystal LiNi_{0.8}Co_{0.1}Mn_{0.1}O₂ with enhanced cycling performances as cathode material for lithium-ion batteries. *Nano Research* <https://doi.org/10.1007/s12274-021-3784-2> (2021).
46. Lv, C. et al. 1D Nb-doped LiNi_{1/3}Co_{1/3}Mn_{1/3}O₂ nanostructures as excellent cathodes for Li-ion battery. *Electrochimica Acta* **297**, 258–266 (2019).
47. Lin, L., Zhang, L., Wang, S., Kang, F. & Li, B. Micro- and nano-structural design strategies towards polycrystalline nickel-rich layered cathode materials. *J. Mater. Chem. A* <https://doi.org/10.1039/D3TA00320E> (2023).
48. Tang, Y., Zhang, Y., Li, W., Ma, B. & Chen, X. Rational material design for ultrafast rechargeable lithium-ion batteries. *Chem. Soc. Rev.* **44**, 5926–5940 (2015).
49. He, X., Sun, H., Ding, X. & Zhao, K. Grain boundaries and their impact on Li kinetics in layered-oxide cathodes for Li-ion batteries. *J. Phys. Chem. C* **125**, 10284–10294 (2021).
50. Zhang, R., Wang, C., Ge, M. & Xin, H. L. Accelerated degradation in a quasi-single-crystalline layered oxide cathode for lithium-ion batteries caused by residual grain boundaries. *Nano Lett.* **22**, 3818–3824 (2022).
51. Nomura, Y., Yamamoto, K., Hirayama, T., Igaki, E. & Saitoh, K. Visualization of lithium transfer resistance in secondary particle cathodes of bulk-type solid-state batteries. *ACS Energy Lett.* **5**, 2098–2105 (2020).
52. Quinn, A. et al. Electron backscatter diffraction for investigating lithium-ion electrode particle architectures. *Cell Rep. Phys. Sci.* **1**, 100137 (2020).
53. Fink, K. et al. Application of electron backscatter diffraction techniques to quantify effects of aging on sub-grain and spatial heterogeneity in NMC cathodes. *Energy Stor. Mater.* **44**, 342–352 (2022).
54. Gu, H. et al. Self-assembled porous LiNi_{0.8}Co_{0.1}Mn_{0.1}O₂ cathode materials with micro/nano-layered hollow morphologies for high-power lithium-ion batteries. *Appl. Surf. Sci.* **539**, <https://doi.org/10.1016/j.apsusc.2020.148034> (2021).
55. Azhari, L. et al. Underlying limitations behind impedance rise and capacity fade of single crystalline Ni-rich cathodes synthesized via a molten-salt route. *J. Power Sources* **545**, <https://doi.org/10.1016/j.jpowsour.2022.231963> (2022).
56. Zhang, Y., Liu, J. & Cheng, F. Concentration-gradient LiNi_{0.85}Co_{0.12}Al_{0.03}O₂ cathode assembled with primary particles for rechargeable lithium-ion batteries. *Energy Fuels* **35**, 13474–13482 (2021).
57. Qiu, L. et al. The structure-activity relationship between precursor fine structure and cathode performance in ultra-high Ni layered oxide. *Chem. Eng. Sci.* **260**, 117865 (2022).
58. Shi, J.-L. et al. Size controllable single-crystalline Ni-rich cathodes for high-energy lithium-ion batteries. *Natl Sci. Rev.* **10**, <https://doi.org/10.1093/nsr/nwac226> (2022).
59. He, Y.-Y. et al. Ni-rich LiNi_{0.6}Co_{0.2}Mn_{0.2}O₂ microrod with hierarchical structure synthesized by template reaction as cathode material for lithium-ion battery. *Ionics* **25**, 5277–5285 (2019).
60. Ryu, W.-H., Lim, S.-J., Kim, W.-K. & Kwon, H. 3-D dumbbell-like LiNi_{1/3}Mn_{1/3}Co_{1/3}O₂ cathode materials assembled with nano-building blocks for lithium-ion batteries. *J. Power Sources* **257**, 186–191 (2014).
61. Wu, Z. et al. Improving electrochemical performance of NCM811 cathodes for lithium-ion batteries via consistently arranging the hexagonal nanosheets with exposed {104} facets. *Ceram. Int.* **48**, 17279–17288 (2022).
62. Park, G.-T., Ryu, H.-H., Noh, T.-C., Kang, G.-C. & Sun, Y.-K. Microstructure-optimized concentration-gradient NCM cathode for long-life Li-ion batteries. *Materials Today* **52**, 9–18 (2022).
63. Noh, H.-J., Yoon, S., Yoon, C. S. & Sun, Y.-K. Comparison of the structural and electrochemical properties of layered Li[NixCoyMnz]O₂ (x = 1/3, 0.5, 0.6, 0.7, 0.8 and 0.85) cathode material for lithium-ion batteries. *J. Power Sources* **233**, 121–130 (2013).
64. Wang, Z. et al. Hierarchical LiNi_{0.8}Co_{0.15}Al_{0.05}O₂ plates with exposed {010} active planes as a high performance cathode material for Li-ion batteries. *RSC Adv.* **6**, 32365–32369 (2016).
65. Zhou, H. et al. Superior stability and dynamic performance of single crystal LiNi_{1/3}Co_{1/3}Mn_{1/3}O₂ nanorods from β-MnO₂ template for lithium-ion batteries. *J. Electrochem. Soc.* **166**, A59–A67 (2019).
66. Chen, Z., Guo, F. & Zhang, Y. Micron-sized monodisperse particle LiNi_{0.6}Co_{0.2}Mn_{0.2}O₂ derived by oxalate solvothermal process combined with calcination as cathode material for lithium-ion batteries. *Materials* **14**, 2576 (2021).
67. Li, F. et al. A nanorod-like Ni-rich layered cathode with enhanced Li⁺ diffusion pathways for high-performance lithium-ion batteries. *J. Mater. Chem. A* **9**, 2830–2839 (2021).
68. Tao, Z., Liu, G., Li, S., Yao, M. & Zhang, Y. Rational structure of rod-like single crystal LiNi_{0.9}Co_{0.05}Mn_{0.04}Al_{0.01}O₂ cathode for superior-stable lithium-ion battery. *Electrochim. Acta* **444**, 141975 (2023).
69. Qian, G. et al. Single-crystal nickel-rich layered-oxide battery cathode materials: synthesis, electrochemistry, and intra-granular fracture. *Energy Stor. Mater.* **27**, 140–149 (2020).
70. Fu, F. et al. Synthesis of single crystalline hexagonal nanobricks of LiNi_{1/3}Co_{1/3}Mn_{1/3}O₂ with high percentage of exposed {010} active facets as high

- rate performance cathode material for lithium-ion battery. *J. Mater. Chem. A* **1**, 3860–3864, (2013).
71. Zhu, J. et al. Atomic-level understanding of surface reconstruction based on Li[Ni_xMn_yCo_{1-x-y}]O₂ single-crystal studies. *ACS Appl. Energy Mater.* **3**, 4799–4811 (2020).
 72. Qian, G. et al. Temperature-swing synthesis of large-size single-crystal LiNi_{0.6}Mn_{0.2}Co_{0.2}O₂ cathode materials. *J. Electrochem. Soc.* **168**, <https://doi.org/10.1149/1945-7111/abde0> (2021).
 73. Lee, S.-H., Sim, S.-J., Jin, B.-S. & Kim, H.-S. High performance well-developed single crystal LiNi_{0.91}Co_{0.06}Mn_{0.03}O₂ cathode via LiCl-NaCl flux method. *Mater. Lett.* **270**, 127615 (2020).
 74. Kimijima, T., Zettsu, N. & Teshima, K. Growth manner of octahedral-shaped Li(Ni_{1/3}Co_{1/3}Mn_{1/3})O₂ single crystals in molten Na₂SO₄. *Cryst. Growth Des.* **16**, 2618–2623 (2016).
 75. Leng, J. et al. Highly-dispersed submicrometer single-crystal nickel-rich layered cathode: spray synthesis and accelerated lithium-ion transport. *Small* **17**, 2006869 (2021).
 76. Lu, Y., Zhu, T., McShane, E., McCloskey, B. D. & Chen, G. Single-crystal LiNi_xMn_yCo_{1-x-y}O₂ cathodes for extreme fast charging. *Small* **18**, 2105833 (2022).
 77. García, J. C. et al. Surface structure, morphology, and stability of Li(Ni_{1/3}Mn_{1/3}Co_{1/3})O₂ cathode material. *J. Phys. Chem. C* **121**, 8290–8299 (2017).
 78. Kan, W. H. et al. Understanding the effect of local short-range ordering on lithium diffusion in Li_{1.3}Nb_{0.3}Mn_{0.4}O₂ single-crystal cathode. *Chem* **4**, 2108–2123 (2018).
 79. Kim, M. et al. Improving LiNiO₂ cathode performance through particle design and optimization. *J. Mater. Chem. A* **10**, 12890–12899 (2022).
 80. Wang, C. et al. Single crystal cathodes enabling high-performance all-solid-state lithium-ion batteries. *Energy Stor. Mater.* **30**, 98–103 (2020).
 81. Kim, A. Y. et al. An elastic carbon layer on echeveria-inspired SnO₂ anode for long-cycle and high-rate lithium ion batteries. *Carbon* **94**, 539–547 (2015).
 82. Yin, S. et al. Fundamental and solutions of microcrack in Ni-rich layered oxide cathode materials of lithium-ion batteries. *Nano Energy* **83**, 105854 (2021).
 83. Jiang, M., Danilov, D. L., Eichel, R. A. & Notten, P. H. L. A Review of degradation mechanisms and recent achievements for Ni-rich cathode-based Li-ion batteries. *Adv. Energy Mater.* **11**, <https://doi.org/10.1002/aenm.202103005> (2021).
 84. Heenan, T. M. M. et al. Identifying the origins of microstructural defects such as cracking within Ni-rich NMC811 cathode particles for lithium-ion batteries. *Adv. Energy Mater.* **10**, <https://doi.org/10.1002/aenm.202002655> (2020).
 85. Wang, B. & Aifantis, K. E. Probing the effect of surface parameters and particle size in the diffusion-induced stress of electrodes during lithium insertion. *Int. J. Mech. Sci.* **215**, <https://doi.org/10.1016/j.ijmeccsci.2021.106917> (2022).
 86. Cheng, Y.-T. & Verbrugge, M. W. The influence of surface mechanics on diffusion induced stresses within spherical nanoparticles. *J. Appl. Phys.* **104**, <https://doi.org/10.1063/1.3000442> (2008).
 87. Minnmann, P. et al. Designing cathodes and cathode active materials for solid-state batteries. *Adv. Energy Mater.* **12**, <https://doi.org/10.1002/aenm.202201425> (2022).
 88. Park, K.-J. et al. Improved cycling stability of Li[Ni_{0.90}Co_{0.05}Mn_{0.05}]O₂ through microstructure modification by boron doping for Li-ion batteries. *Adv. Energy Mater.* **8**, 1801202 (2018).
 89. Sun, H. H., Dolocan, A., Weeks, J. A., Heller, A. & Mullins, C. B. Stabilization of a highly Ni-rich layered oxide cathode through flower-petal grain arrays. *ACS Nano* **14**, 17142–17150 (2020).
 90. Li, Y. et al. Tungsten-consolidated crystal structure of LiNi_{0.6}Co_{0.2}Mn_{0.2}O₂ cathode materials for superior electrochemical performance. *Appl. Surface Sci.* **509**, 145287 (2020).
 91. Kim, U.-H. et al. High-energy W-doped Li[Ni_{0.95}Co_{0.04}Al_{0.01}]O₂ cathodes for next-generation electric vehicles. *Energy Stor. Mater.* **33**, 399–407 (2020).
 92. Ryu, H. H. et al. Li[Ni_{0.9}Co_{0.09}W_{0.01}]O₂: a new type of layered oxide cathode with high cycling stability. *Adv. Energy Mater.* **9**, <https://doi.org/10.1002/aenm.201902698> (2019).
 93. Park, G.-T., Ryu, H.-H., Park, N.-Y., Yoon, C. S. & Sun, Y.-K. Tungsten doping for stabilization of Li[Ni_{0.90}Co_{0.05}Mn_{0.05}]O₂ cathode for Li-ion battery at high voltage. *J. Power Sources* **442**, 227242 (2019).
 94. Park, G.-T. et al. Ultrafine-grained Ni-rich layered cathode for advanced Li-ion batteries. *Energy Environ. Sci.* **14**, 6616–6626 (2021).
 95. Kim, U. H. et al. Microstructure engineered Ni-rich layered cathode for electric vehicle batteries. *Adv. Energy Mater.* **11**, 2100884 (2021). n/a.
 96. Ryu, H.-H. et al. Capacity fading mechanisms in Ni-rich single-crystal NCM cathodes. *ACS Energy Lett.* **6**, 2726–2734 (2021).
 97. Tongchao, L. et al. Rational design of mechanically robust Ni-rich cathode materials via concentration gradient strategy. *Nat. Commun.* **12**, 6024–6024 (2021).
 98. Sun, Y.-K., Myung, S.-T., Kim, M.-H., Prakash, J. & Amine, K. Synthesis and characterization of Li[(Ni_{0.8}Co_{0.1}Mn_{0.1})_{0.8}(Ni_{0.5}Mn_{0.5})_{0.2}]O₂ with the microscale core–shell structure as the positive electrode material for lithium batteries. *J. Am. Chem. Soc.* **127**, 13411–13418 (2005).
 99. Kim, J. et al. Prospect and reality of Ni-rich cathode for commercialization. *Adv. Energy Mater.* **8**, <https://doi.org/10.1002/aenm.201702028> (2018).
 100. Sun, Y.-K. et al. High-energy cathode material for long-life and safe lithium batteries. *Nat. Mater.* **8**, 320–324 (2009).
 101. Lim, B.-B. et al. Advanced concentration gradient cathode material with two-slope for high-energy and safe lithium batteries. *Adv. Funct. Mater.* **25**, 4673–4680 (2015).
 102. Noh, H.-J. et al. Cathode material with nanorod structure—an application for advanced high-energy and safe lithium batteries. *Chem. Mater.* **25**, 2109–2115 (2013).
 103. Myung, S. T., Noh, H. J., Yoon, S. J., Lee, E. J. & Sun, Y. K. Progress in high-capacity core-shell cathode materials for rechargeable lithium batteries. *J. Phys. Chem. Lett.* **5**, 671–679 (2014).
 104. Yoon, C. S. et al. Microstructure evolution of concentration gradient Li[Ni_{0.75}Co_{0.10}Mn_{0.15}]O₂ cathode for lithium-ion batteries. *Adv. Funct. Mater.* **28**, 1802090 (2018). n/a.
 105. Hou, P., Zhang, H., Zi, Z., Zhang, L. & Xu, X. Core-shell and concentration-gradient cathodes prepared via co-precipitation reaction for advanced lithium-ion batteries. *J. Mater. Chem. A, Mater. Energy Sustain.* **5**, 4254–4279 (2017).
 106. Yang, X. et al. Tailoring structure of Ni-rich layered cathode enable robust calendar life and ultrahigh rate capability for lithium-ion batteries. *Electrochim. Acta* **320**, 134587 (2019).
 107. Koshika, Y., Kaneda, H., Yoshio, S. & Furuichi, Y. Precursor morphology control and electrochemical properties of LiNi_{0.35}Mn_{0.30}Co_{0.35}O₂ as a Li-ion battery positive electrode material. *ACS Appl. Energy Mater.* <https://doi.org/10.1021/acsaem.2c00698> (2022).
 108. Li, J., Xiong, S., Liu, Y., Ju, Z. & Qian, Y. Uniform LiNi_{1/3}Co_{1/3}Mn_{1/3}O₂ hollow microspheres: designed synthesis, topotactical structural transformation and their enhanced electrochemical performance. *Nano Energy* **2**, 1249–1260 (2013).
 109. Müller, M., Schneider, L., Bohn, N., Binder, J. R. & Bauer, W. Effect of nanostructured and open-porous particle morphology on electrode processing and electrochemical performance of Li-ion batteries. *ACS Appl. Energy Mater.* **4**, 1993–2003 (2021).
 110. Song, J., Kim, J., Kang, T. & Kim, D. Design of a porous cathode for ultrahigh performance of a Li-ion battery: an overlooked pore distribution. *Sci. Rep.* **7**, 42521 (2017). **The effects of 3D porous structures on the capacity of cathode particles with different C-rate have been studied in both theoretical simulation and experiments.**
 111. Ren, D. et al. Ultrahigh rate performance of a robust lithium nickel manganese cobalt oxide cathode with preferentially oriented Li-diffusing channels. *ACS Appl. Mater. Interfaces* **11**, 41178–41187 (2019).
 112. Liu, Y., Lv, P., Ma, J., Bai, R. & Duan, H. L. Stress fields in hollow core–shell spherical electrodes of lithium ion batteries. *Proc. R. Soc. A: Math. Phys. Eng. Sci.* **470**, <https://doi.org/10.1098/rspa.2014.0299> (2014).
 113. Ma, X. et al. Recycled cathode materials enabled superior performance for lithium-ion batteries. *Joule* <https://doi.org/10.1016/j.joule.2021.09.005> (2021).
 114. Cha, H. et al. Boosting reaction homogeneity in high-energy lithium-ion battery cathode materials. *Adv. Mater.* **32**, e2003040 (2020).
 115. Tan, Z. et al. One-dimensional hierarchical porous layered oxide LiNi_{0.8}Co_{0.1}Mn_{0.1}O₂ cathode for lithium-ion batteries via self-template interstitial co-precipitation method. *Chem. Lett.* **50**, 1385–1387 (2021).
 116. Wu, N. et al. Facile synthesis of one-dimensional LiNi_{0.8}Co_{0.15}Al_{0.05}O₂ microrods as advanced cathode materials for lithium ion batteries. *J. Mater. Chem. A* **3**, 13648–13652 (2015).
 117. Cheng, Q., Yang, T., Li, M. & Chan, C. K. Exfoliation of LiNi_{1/3}Mn_{1/3}Co_{1/3}O₂ into nanosheets using electrochemical oxidation and reassembly with dialysis or flocculation. *Langmuir* **33**, 9271–9279 (2017).
 118. Zou, Y. et al. Multishelled Ni-rich Li(Ni_xCoyMnz)O₂ hollow fibers with low cation mixing as high-performance cathode materials for Li-ion batteries. *Adv. Sci.* **4**, 1600262 (2017).
 119. Stein, P. & Xu, B. 3D isogeometric analysis of intercalation-induced stresses in Li-ion battery electrode particles. *Comput. Method. Appl. Mech. Eng.* **268**, 225–244 (2014).
 120. Deshpande, R., Cheng, Y.-T. & Verbrugge, M. W. Modeling diffusion-induced stress in nanowire electrode structures. *J. Power Sources* **195**, 5081–5088 (2010).
 121. Zhang, J., Qiao, J., Sun, K. & Wang, Z. Balancing particle properties for practical lithium-ion batteries. *Particuology* **61**, 18–29 (2022).
 122. Li, W. et al. Dynamic behaviour of interphases and its implication on high-energy-density cathode materials in lithium-ion batteries. *Nat. Commun.* **8**, 14589–14589 (2017).
 123. Namkoong, B. et al. High-energy Ni-rich cathode materials for long-range and long-life electric vehicles. *Adv. Energy Mater.* **12**, 2200615 (2022).

124. Rajagopal, R., Subramanian, Y. & Ryu, K. S. Improving the electrochemical performance of cathode composites using different sized solid electrolytes for all solid-state lithium batteries. *RSC Adv.* **11**, 32981–32987 (2021).
125. Froboese, L., Sichel, J. F. V. D., Loellhoeffel, T., Helmers, L. & Kwade, A. Effect of microstructure on the ionic conductivity of an all solid-state battery electrode. *J. Electrochem. Soc.* **166**, A318–A328 (2019).
126. Jeon, H. et al. Tailoring shape and exposed crystal facet of single-crystal layered-oxide cathode particles for all-solid-state batteries. *Chem. Eng. J.* **445**, <https://doi.org/10.1016/j.cej.2022.136828> (2022).
127. Montoya, A. T. et al. Direct recycling of lithium-ion battery cathodes: a multi-stage annealing process to recover the pristine structure and performance. *ACS Sustain. Chem. Eng.* **10**, 13319–13324 (2022).
128. Ma, X. et al. Direct upcycling of mixed Ni-lean polycrystals to single-crystal Ni-rich cathode materials. *Chem* **8**, 1944–1955 (2022).
129. Zheng, Y. et al. The effects of phosphate impurity on recovered LiNi_{0.6}Co_{0.2}Mn_{0.2}O₂ cathode material via a hydrometallurgy method. *ACS Applied Materials & Interfaces* **14**, 48627–48635 (2022).
130. Chen, M. et al. Recycling end-of-life electric vehicle lithium-ion batteries. *Joule* **3**, 2622–2646 (2019).
131. Sloop, S. E. et al. Cathode healing methods for recycling of lithium-ion batteries. *Sustain. Mater. Technol.* **22**, <https://doi.org/10.1016/j.susmat.2019.e00113> (2019).
132. Shi, Y., Chen, G., Liu, F., Yue, X. & Chen, Z. Resolving the compositional and structural defects of degraded LiNi_xCoyMnzO₂ particles to directly regenerate high-performance lithium-ion battery cathodes. *ACS Energy Lett.* **3**, 1683–1692 (2018).
133. Shi, Y., Zhang, M., Meng, Y. S. & Chen, Z. Ambient-pressure relithiation of degraded Li_xNi_{0.5}Co_{0.2}Mn_{0.3}O₂ (0 < x < 1) via eutectic solutions for direct regeneration of lithium-ion battery cathodes. *Adv. Energy Mater.* **9**, 1900454 (2019).
134. Zhang, X. et al. Sustainable recycling and regeneration of cathode scraps from industrial production of lithium-ion batteries. *ACS Sustain. Chem. Eng.* **4**, 7041–7049 (2016).
135. Yang, Q. et al. Ionic liquids and derived materials for lithium and sodium batteries. *Chem. Soc. Rev.* **47**, 2020–2064 (2018).
136. Ganter, M. J., Landi, B. J., Babbitt, C. W., Anctil, A. & Gaustad, G. Cathode refunctionalization as a lithium ion battery recycling alternative. *J. Power Sources* **256**, 274–280 (2014).
137. Park, G.-T. et al. Introducing high-valence elements into cobalt-free layered cathodes for practical lithium-ion batteries. *Nat. Energy* **7**, 946–954 (2022).
138. Qian, G. et al. Value-creating upcycling of retired electric vehicle battery cathodes. *Cell Rep. Phys. Sci.* **3**, 100741 (2022).
139. Zhou, H., Zhao, X., Yin, C. & Li, J. Regeneration of LiNi_{0.5}Co_{0.2}Mn_{0.3}O₂ cathode material from spent lithium-ion batteries. *Electrochim. Acta* **291**, 142–150 (2018).
140. Li, J. et al. Regenerating of LiNi_{0.5}Co_{0.2}Mn_{0.3}O₂ cathode materials from spent lithium-ion batteries. *J. Mater. Sci. Mater. Electron.* **29**, 17661–17669 (2018).
141. Zhang, R. et al. Understanding fundamental effects of Cu impurity in different forms for recovered LiNi_{0.6}Co_{0.2}Mn_{0.2}O₂ cathode materials. *Nano Energy* **78**, 105214 (2020).
142. Kim, U.-H. et al. Microstructure-controlled Ni-rich cathode material by microscale compositional partition for next-generation electric vehicles. *Adv. Energy Mater.* **9**, 1803902 (2019).
143. Su, Y. et al. Improved stability of layered and porous nickel-rich cathode materials by relieving the accumulation of inner stress. *ChemSusChem* **13**, 426–433 (2020).
144. Mao, Y. et al. High-voltage charging-induced strain, heterogeneity, and micro-cracks in secondary particles of a nickel-rich layered cathode material. *Adv. Funct. Mater.* **29**, 1900247 (2019). **This study shows that cathode with hollow morphology is more robust against stress inside particles than that of particles with solid inner.**
145. Fan, X. et al. Crack-free single-crystalline Ni-rich layered NCM cathode enable superior cycling performance of lithium-ion batteries. *Nano Energy* **70**, <https://doi.org/10.1016/j.nanoen.2020.104450> (2020). **Through comparing the cycle performance of single crystal and polycrystal cathode materials, this study illustrates that single crystal particles are better than polycrystal particles in the field of preventing the crack generation and side reactions.**
146. Yu, X. et al. Achieving low-temperature hydrothermal relithiation by redox mediation for direct recycling of spent lithium-ion battery cathodes. *Energy Stor. Mater.* **51**, 54–62 (2022).
147. Wang, T. et al. Direct recycling of spent NCM cathodes through ionothermal lithiation. *Adv. Energy Mater.* **10**, <https://doi.org/10.1002/aenm.202001204> (2020).

Author contributions

Z.M. and X.M. led the conceptualization and wrote the original manuscript. L.A. revised the manuscript. J.H. prepared the figures and tables. Y.W. supervised, reviewed, and edited the paper.

Competing interests

The authors declare no competing interests.

Additional information

Correspondence and requests for materials should be addressed to Yan Wang.

Peer review information *Communications Materials* thanks the anonymous reviewers for their contribution to the peer review of this work. Primary handling editor: Jet-Sing Lee.

Reprints and permission information is available at <http://www.nature.com/reprints>

Publisher's note Springer Nature remains neutral with regard to jurisdictional claims in published maps and institutional affiliations.



Open Access This article is licensed under a Creative Commons Attribution 4.0 International License, which permits use, sharing, adaptation, distribution and reproduction in any medium or format, as long as you give appropriate credit to the original author(s) and the source, provide a link to the Creative Commons licence, and indicate if changes were made. The images or other third party material in this article are included in the article's Creative Commons licence, unless indicated otherwise in a credit line to the material. If material is not included in the article's Creative Commons licence and your intended use is not permitted by statutory regulation or exceeds the permitted use, you will need to obtain permission directly from the copyright holder. To view a copy of this licence, visit <http://creativecommons.org/licenses/by/4.0/>.

© The Author(s) 2023